

Temporary Anion Resonances of Pyrene: a 2D Photoelectron Imaging and Computational Study

Aude Lietard†, Jan R. R. Verlet†, Stephen Slimak‡, Kenneth D. Jordan‡**

†Department of Chemistry, Durham University, Durham DH1 3LE, United Kingdom

‡Department of Chemistry, University of Pittsburgh, Pittsburgh, PA 15260 USA

Abstract

The low energy electron scattering resonances of pyrene have been characterized using experimental and computational methods. Experimentally, 2D PE imaging of the pyrene anion was used to probe the dynamics of resonances over the first 4 eV of the continuum. Computationally, the energies and character of the anion states were determined using equation-of-motion coupled cluster calculations while taking specific care to avoid the collapse onto discretised continuum levels and application of the pairing theorem. Our results are in good agreement with the predictions of electron-scattering calculations that included an offset and with the pyrene anion absorption spectrum in a glass matrix. Taken together, we offer an assignment of the first five electronic resonances of pyrene. Some of the population in the lowest energy ${}^2B_{1u}$ resonance was observed to decay to the ground electronic state of the anion, while all other resonances decay by direct autodetachment. The astronomical relevance of ground state electron capture of a low energy resonance in pyrene is discussed.

* j.r.r.verlet@durham.ac.uk

* jordan@pitt.edu

Introduction

Pyrene ($C_{16}H_{10}$, Figure 1(a)) is a small polycyclic aromatic hydrocarbon (PAH) consisting of four fused benzene rings that is found throughout nature and has numerous technological uses that stem from its photophysical properties that arise from the delocalised π -system. Pyrene is an interesting case of an aromatic system that does not obey the $4n + 2$ Hückel rule.^{1,2} The first observation of intermolecular excimer emission was in pyrene solutions,³ and this has led to its ubiquitous use as fluorescent probes for microenvironmental perturbations and sensing.^{4,5} Pyrene has also found extensive application in molecular electronics,⁶ where its derivatives serve as organic materials in the active components of devices. In nature, pyrene and other PAHs are formed in many pyrolytic processes. In the interstellar medium, PAHs are thought to be responsible for the diffuse interstellar bands (DIBs)^{7,8} and pyrene has been observed in molecular clouds,⁹ which are the chemical reaction flasks of the interstellar medium where complex molecules are formed often through the interaction with photons or electrons.⁷ Based on the above, it comes as no surprise that the photophysical properties of pyrene have been the subject of numerous studies. In contrast, the anion of pyrene, $C_{16}H_{10}^-$, has received far less attention and, to the best of our knowledge, there are no systematic experimental studies of its electronic resonances in the gas phase. This is surprising because the redox properties of pyrene are important from a molecular electronics perspective and because chemistry in the interstellar medium is often initiated by low energy electrons.

The ground state anion of pyrene is known to be bound,¹⁰ but all of the excited states of the anion are expected to be unbound, hence, to lie energetically above the ground state of the neutral molecule. As a result, the excited anion states are temporary in nature, being subject to electron detachment, and thus would appear as resonances using electron scattering methods such as electron transmission and electron energy loss spectroscopy.^{11–14} In particular, two-dimensional (2D) electron energy loss spectroscopy is an insightful method to probe the dynamics of anion resonances.^{15–17} In this approach, the electron energy is scanned across the continuum and, at each incident kinetic energy of the electron, a spectrum of the outgoing electron kinetic energy (eKE) is recorded. Dynamics occurring in a temporary anion resonance can then be identified by changes in eKE. A recent addition to the experimental arsenal for probing electron-molecule resonances is anion 2D photoelectron (PE) spectroscopy.^{18,19} This is similar in spirit to 2D electron energy loss spectroscopy, but starts from the bound ground state anion and uses a photon to access the anion resonances. As the resonances are unbound, the process is anion PE spectroscopy, where

the PE spectrum at each photon energy ($h\nu$) contains signatures of resonance dynamics. For molecules with similar anion and neutral ground state geometries, the method provides resonance positions in close agreement with those from electron scattering measurements on the neutral molecule and contain similar information concerning the dynamics leading to electron emission.²⁰ This is the case for PAHs, as recently demonstrated in anthracene, which showed a close correlation with electron-scattering experiments.²¹

For pyrene, no electron scattering experiments have been reported. The ground state anion of pyrene is stable with an adiabatic electron affinity of 0.41 eV¹⁰ and can be made in a molecular beam source by secondary electron attachment. Ando *et al.*¹⁰ and Kim *et al.*²² have used PE spectroscopy to investigate the anionic clusters of pyrene. As part of their studies, both groups presented PE spectra of $C_{16}H_{10}^-$ at a number of different wavelengths. These showed changes in the Franck-Condon profile between different spectra and provided evidence for delayed or autodetachment at 3.49 eV. However, probing such changes in isolation (i.e., at well-separated $h\nu$ that access very different regions of the continuum) does not offer much insight onto the dynamics or locations of the resonances. There are a number of transitions that can be excited in the anion, as identified by the optical absorption spectrum of $C_{16}H_{10}^-$ in a cryogenic matrix,^{23,24} and some of these coincide with the wavelengths used in the PE spectra. Hence, 2D PE spectroscopy is well-suited to delineate the spectral changes arising from excitation to specific resonances.

Computational characterization of electron-scattering resonances of polyatomic molecules is a challenging problem. Both scattering and electronic structure methods can be employed, but in the former case there is the challenge of adequate treatment of polarization, correlation, and exchange effects, and in the latter case one has to account for the fact that temporary anion states are embedded in the continuum of the neutral molecule plus a free electron and to avoid the collapse of the wave function to the neutral molecules plus a discretized continuum orbital.²⁵ Singh *et al.* have recently used the R-matrix method to study electron scattering from pyrene with incident electron energies between 0.1 and 15 eV,²⁶ and they observed a number of resonances in this range, although, as we discuss below, the energies that they obtain for the anion states are too high by about 1 eV.

In the present study, we present a combined experimental and computational investigation on the low energy resonances of pyrene. Experimentally, we employ 2D PE imaging and computationally, we determine energies of the anion states using electronic structure approaches that avoids the collapse onto discretised continuum levels.

Methods

Experimental

The 2D PE spectroscopy was performed using an anion PE imaging spectrometer that is equipped with a molecular beam source that has been described in detail elsewhere.²⁷ Briefly, solid pyrene (Sigma Aldrich) was heated in a pulsed valve to 185 °C and its vapour pressure was co-expanded with 3 bar of Ar backing gas into vacuum (10^{-5} mbar) at 10 Hz. At the throat of the expansion, the molecular beam was crossed by a 300 eV electron beam. The resulting gas mixture entered between the plates of a Wiley-Maclaren mass spectrometer,²⁸ where anions were accelerated down a time-of-flight drift tube. At the focus of the mass-spectrometer, mass-selected anions interacted with light pulses at the centre of a velocity map imaging PE spectrometer.²⁹ Liberated electrons were captured on a gated position-sensitive detector and impacts monitored using a CMOS camera. The gating only allows for electrons in a ~ 200 ns window to be collected. Raw images were acquired to achieve a broadly similar signal level between different photon energies and ranged from $\sim 10^3$ to 10^4 laser shots. Light pulses at 10 Hz were generated using a Nd:YAG-pumped optical parametric oscillator (OPO) (Continuum Surelite and Horizon) producing pulses of ~ 5 ns duration. The photon energy of the OPO was scanned from $0.6 \leq h\nu \leq 4.5$ eV (corresponding to 2066 to 276 nm). PE spectra were obtained from the raw images using the polar onion peeling algorithm³⁰ and were calibrated using the known PE spectrum of I^- . The spectral resolution of the PE spectrometer is $\sim 3\%$ of the eKE.

Computational

As described in the Introduction, although the ground state anion of pyrene is bound, the electronically excited anion states are metastable, meaning that they are embedded in the electron detachment continuum. In finite basis set electronic structure calculations the continuum is discretized, yielding so-called discretized continuum (DC) solutions. In a diabatic picture, a temporary anion resonance can be viewed as resulting from the coupling between a discrete state and the continuum.²⁵ With sufficiently small basis sets, the discrete state of a particular symmetry lies energetically below the lowest energy DC, which avoids variational collapse onto the DC level, but with basis sets containing highly diffuse functions, there will be one or more DC levels below the discrete state and standard electronic structure calculations will collapse onto a DC level. This issue is particularly problematical since diffuse basis functions are required for accurately determining the absolute values of the energies of temporary anions and

they are essential for calculating the lifetimes. Multiple strategies have been developed to deal with the collapse onto continuum problem when using flexible basis sets. These include the stabilization method,³¹ the complex absorbing potential (CAP),^{32,33} the coordinate rotation method,^{34,35} and complex basis function approaches.³⁶ However, here we are primarily interested in estimating the relative energies of the low-lying anion states of pyrene, rather than the absolute energies and widths (proportional to the reciprocals of the lifetimes). For this purpose, we employed the equation-of-motion coupled cluster singles doubles (EOM-CCSD) method for electron affinities³⁷ together with the cc-pVTZ-*f/d* basis set, formed from the cc-pVTZ basis set³⁸ by omitting the *f* functions on the C atoms and the *d* functions on the H atoms. We checked to establish that the DC levels of the relevant symmetries are sufficiently high in energy as to avoid the variational collapse problem. In addition, we also carried out stabilization calculations using the EOM-CCSD method and the cc-pVTZ-*f/d* basis set augmented with a diffuse *p* function on each carbon atom, with the exponent of the diffuse function being scaled. For the five lowest energy anions states the stabilization calculations gave electron affinities to within 0.1 eV of those obtained from the calculations in the cc-pVDZ-*f/d* basis set without stabilization. Thus, only the latter results are reported here.

The geometry of the ground state of the neutral molecule was optimized using the B3LYP density functional method³⁹⁻⁴² together with the 6-31G(d) basis set.⁴³ Pyrene has D_{2h} symmetry, and in our treatment, the molecule lies in the *xy* plane with the long axis in the *y* direction, as shown in Figure 1(a). The geometry optimization was carried using Gaussian 16,⁴⁴ and the EOM calculations were carried out using the CFOUR code.⁴⁵

Pyrene is an alternant hydrocarbon, and, as such, one would expect that the energies of the low-lying π^* anion states could be predicted in a semiquantitative manner using the pairing theorem.⁴⁶⁻⁴⁸ According to the pairing theorem, the energies of the filled π and empty π^* orbitals are related as follows:

$$\epsilon_{\text{HOMO}-i} + \epsilon_{\text{LUMO}+i} = \text{constant} \quad (1)$$

where $i = 0$ denotes the frontier orbitals, i.e., the highest occupied molecular orbital (HOMO) and lowest unoccupied molecular orbital (LUMO). This result rigorously holds in the Hückel approximation with nearest neighbor interactions only and neglecting explicit treatment of orbital overlap. Although it does not rigorously hold in a many-

electron treatment of electronic structure, it has been found to approximately hold when using experimental values of the π ionization potentials (IPs) and π^* electron affinities (EAs), i.e.,

$$\text{IP}_i + \text{EA}_j = \text{constant} \quad (2)$$

in the case that the IPs and EAs in question are predominantly single particle in nature. In Eq. 2, i denotes the orbitals in question, numbered as described above, and the constant differs from that in Eq. 1. Equation 2 has also been found to approximately hold for other alternant hydrocarbons when using theoretical methods that avoid the collapse of the anion resonances onto the continuum problem, and it is of interest to determine whether this is the case for pyrene as well. Using experimental values of the first IP⁴⁹ and EA⁵⁰ of benzene, one obtains a value of 8.0 eV for the constant in Eq. 2.

Results

Figure 1(b) shows the 2D PE spectrum of $\text{C}_{16}\text{H}_{10}^-$ in the energy range $0.6 \leq h\nu \leq 4.5$ eV, constructed from 75 PE spectra taken at 50 meV intervals from $1.0 \leq h\nu \leq 4.5$ eV and 100 meV intervals below 1.0 eV (note that the $h\nu$ axis is on the left side of Figure 1(b)). Each PE spectrum has been normalised to its integrated signal to accentuate changes in the spectra with $h\nu$. For direct detachment with no involvement of resonances, the spectrum is determined by the Franck-Condon factors between the ground state anion and various states of the neutral molecule and the electron kinetic energy, eKE, will increase linearly with $h\nu$ (i.e., the binding energy remains constant). Hence, such direct detachment channels will appear as diagonal features in Figure 1(b) with no changes in the spectral shape as $h\nu$ varies. Figure 1(b) shows a number of well-separated diagonal features starting at $h\nu = 0.41, 2.54$ and 3.85 eV, corresponding to electron detachment to different final states of the neutral: namely, the ground state, lowest energy triplet state, and lowest energy singlet state, respectively. From our data, we determine an adiabatic electron affinity (EA) of 0.41 ± 0.01 eV, in excellent agreement with that determined by Ando *et al.*¹⁰ The lowest energy triplet and singlet states of the neutral molecule, $^3\text{B}_{2u}$ and $^1\text{B}_{3u}$, are found to lie energetically 2.13 and 3.44 eV, respectively, above the ground state of the neutral. Both energies are in excellent agreement with the results of previous PE spectra¹⁰ and the latter also being in good agreement with the transition energy of jet-cooled neutral pyrene at 3.37

eV, determined by fluorescence action spectroscopy.^{51,52} Using the EA associated with formation of the ground state anion, we also include a vertical axis indicating the energy above the X^1A_g ground state of the neutral molecule, $h\nu - EA$, which corresponds to the electron energy required to excite specific resonances.

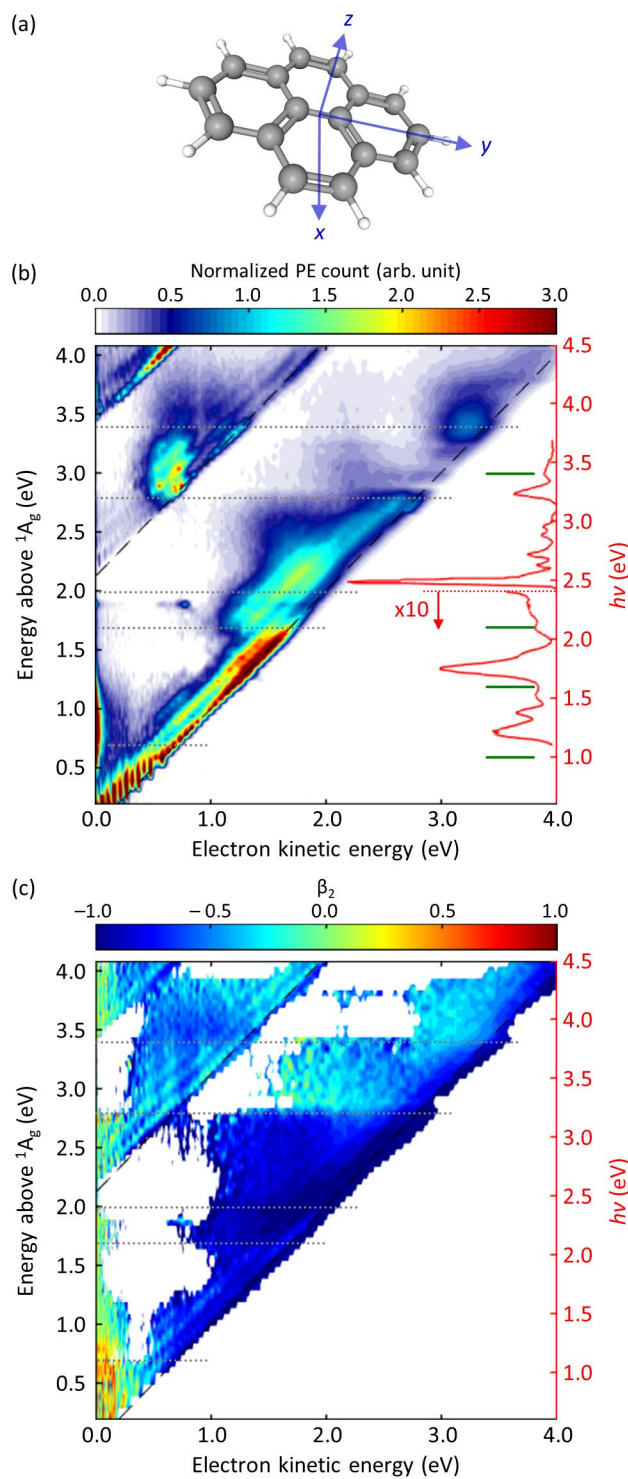


Figure 1: (a) Structure of pyrene including coordinate system used, (b) 2D photoelectron spectrum of the pyrene anion, and (c) 2D photoelectron angular distributions. In (b) and (c) the right vertical axes show the photon energy ($h\nu$) used to obtain the photoelectron spectra. The left axes show the energy above the neutral ground state, X^1A_g ($h\nu - EA$). Also shown in (b) is the absorption spectrum of the pyrene anion in a matrix at 77 K (red curve)²⁴. The positions of computed transitions are indicated as green horizontal lines. The positions of resonances determined from the 2D PE spectrum are shown as grey dashed horizontal lines in (b) and (c). The absorption spectrum in (b) was adapted with permission from ref. 24. Copyright 1973 American Chemical Society.

Although there are clear diagonal features in Figure 1(b), there are also quite dramatic changes in spectral shape and between differing final states as $h\nu$ increases. Such changes generally indicate that the absorption of a photon has transferred population to an anion resonance which autodetaches with different Franck-Condon factors compared to photon absorption leading to the ground state of the neutral plus a free electron (i.e., direct detachment). Such signals often appear as vertical features in the 2D PE spectrum, where vibrational energy imparted upon the excitation of a resonance is preserved upon fast autodetachment.^{18,19} Nuclear motion on the potential energy surface of a resonance can take place before an electron autodetaches, leading to additional changes in the Franck-Condon factors. In extreme cases, non-adiabatic coupling can lead to internal conversion between resonance states or from a resonance state to the electronically bound anion ground state.^{53,54} In this case, the initially imparted energy from the photon remains in the anionic system as vibrational excitation, distributed amongst the internal degrees of freedom (i.e., as heat), and an electron will eventually boil-off. The spectral distribution associated with this thermionic emission is generally peaked at very low eKE with an exponential decay profile and serves as a tell-tale sign of such a process.⁵⁵⁻⁵⁷ Figure 1(b) shows such a signal for $1.0 \leq h\nu \leq 1.5$ eV.

The onset of spectral changes provides a measure of the location of photo-excited resonances, as demonstrated for anthracene.²¹ For pyrene these occur at $h\nu \sim 1.1, 2.1, 2.4, 3.2$ and 3.8 eV; as highlighted on the 2D PE spectrum in Figure 1(b) and tabulated in Table 1. Transitions at $h\nu \sim 1.1, 3.2$ and 3.8 eV are quite easy to identify as they appear to be well-separated from other transitions. The two transitions at $h\nu \sim 2.1$ and 2.4 eV are more difficult to distinguish. There is a clear change in Franck-Condon profile at $h\nu = 2.1$ eV, so this corresponds to one onset. The second can be identified by the vertical PE feature in the $2.5 < h\nu < 3.0$ eV range, which has an onset of $h\nu \sim 2.4$ eV, and will be discussed in more detail below. Naturally, the energies determined in this manner have a substantial uncertainty associated with them, which we estimate to be about ± 0.2 eV. The PE spectrum at $h\nu = 2.30$

eV shows a spurious narrow peak at $eKE \sim 0.8$ eV. This comes about from an unfortunate alignment within the OPO at this specific $h\nu$ that results in both signal and idler beams emerging colinearly from the OPO. With the signal at $h\nu = 2.30$ eV and idler at $h\nu = 1.19$ eV, both these PE spectra appear in the image (with the one at 1.19 eV significantly weaker and having the wrong polarization). Hence, the spurious peak at $eKE \sim 0.8$ eV comes about from detachment by the idler.

Figure 1(c) shows the PE angular distributions quantified by the anisotropy parameter β_2 associated with the 2D PE spectrum. β_2 ranges from +2 to -1 for electrons emitted predominantly parallel and perpendicular to the polarisation axis of the light, respectively.⁵⁸ PE angular distributions are determined by the orbital from which the electron is detached. For s- or σ -type orbitals, β_2 is generally positive, while for p- or π -type orbitals, β_2 is generally negative.⁵⁹⁻⁶¹ PE angular distributions have also been shown to be sensitive to resonances because the orbital from which the electron is removed has changed, and because autodetachment can be preceded by dynamics on the resonance. Resonances therefore typically appear as abrupt changes in β_2 as a function of either $h\nu$ or eKE .^{18,21,62,63} Unfortunately, it is not yet possible to predict such changes and therefore correlate these changes to specific orbitals or dynamics. Nevertheless, they can provide additional support for the observation of resonances seen in the 2D PE spectrum and this is also the case for $C_{16}H_{10}^-$. Overall, for direct detachment channels seen in Figure 1(b), β_2 is negative and approaches -1, as expected for detachment from a π orbital. The location of resonances taken from the 2D PE spectrum is reproduced in Figure 1(c) and clear changes in β_2 can be seen certain for certain resonances. In particular, the resonance at $h\nu = 3.2$ eV is noticeable with the autodetachment feature having a $\beta_2 \sim 0$. Overall, however, the changes for resonances at lower energies are difficult to discern (which may be a reflection that the orbitals involved are all of π -character) and we refrain from commenting and interpreting the PE angular distributions further.

Also included in Figure 1(b) is the absorption spectrum taken by Shida and Iwata, where $C_{16}H_{10}^-$ is generated by γ -ray irradiation of a sample in a 2-methyltetrahydrofuran matrix at 77 K.²⁴ Note that the absorption spectrum may be influenced by the matrix. In particular, given the dielectric constant of the THF matrix, one would expect the first excited anion state of pyrene to be bound in the matrix and that the higher lying excited states, while still being subject to electron autodetachment, to have longer lifetimes than the corresponding resonance states in the gas-phase. The absorption spectrum shows a series of three weak transitions between ~ 1.1 and 2.5 eV. The first peaks at 1.21 eV

and has a vibrational progression. The next transition peaks at 1.75 eV and is about twice as intense, with a third weaker transition appearing at 2.10 eV. This is followed by an intense transition at 2.49 eV with some associated vibrational structure at higher energy. This transition appears quite narrow, and we note that the absorbance below 2.4 eV has been scaled down by an order of magnitude. Beyond this, a final transition can be identified that peaks at 3.23 eV.

The calculations of the excitation energies and electron affinities of the neutral molecule were carried out using the EOM-CCSD method and the cc-pVTZ basis set. These, together with the results of the pairing theorem analysis using the IPs from the pyrene VUV PE spectrum,⁶⁴ form the basis of the assignments of the experimental transitions. The reported calculated excitation energies of the anion were obtained using the optimized geometry of the ground state of the neutral molecule. The excitation energies are impacted by 0.2 eV or less if calculated using the optimized geometry of the anion rather than that of the neutral molecule. We note also that even with the relatively compact cc-pVTZ basis set, the ground state of the anion is predicted to be bound, lying energetically 0.18 eV below the neutral at the same geometry. The experimental value of the vertical detachment energy is 0.41 eV. Table 1 summarizes the calculated and experimental excitation energies of the anion and neutral molecule, along with the assignments of the various transitions (resonances) observed.

Table 1: Transition energies of the pyrene anion from its 2A_u ground state and for the neutral molecule from its X^1A_g ground state. All energies are in eV.

Transition	EOM-CCSD	Absorption spectroscopy	2D PE gas-phase spectroscopy	R-matrix-SEP – 1eV (width) ^c	Pairing theorem ^d
${}^2B_{1u}$	1.0	1.21 ^a	1.1	0.9 (0.06)	0.9
(1) ${}^2B_{3g}$	1.6	1.75 ^a	–	1.5 (0.28)	1.6
${}^2B_{2g}$	2.1	2.10 ^a	2.1	2.0 (0.63)	1.9
${}^2B_{2g}(2p1h)$	–	2.49 ^a	2.4	–	2.6
(2) ${}^2B_{3g}$	3.4	3.23 ^a	3.2	3.5 (0.14)	3.3
?	–	–	3.8	–	–
${}^3B_{2u}$	1.86	–	2.13		
${}^1B_{3u}$		3.37 ^b	3.44		
${}^1B_{2u}$	3.91				

^aTaken from ref²⁴. ^bTaken from ref⁵². ^cEnergies taken from ref²⁶ with 1.0 eV subtracted. ^dDetermined using ionization potentials from Ref⁶⁴.

Figure 2 shows the five lowest energy π^* molecular orbitals of pyrene along with their symmetry labels as well as the dominant configurations of the energetically low-lying electronic states of the anion. The highest occupied molecular orbital (HOMO) of the neutral is of b_{2g} symmetry, and the next most stable occupied orbital (HOMO-1) is of b_{3g} symmetry. The first five π^* orbitals depicted in the figure are of a_u , b_{1u} , b_{3g} , b_{2g} , and b_{3g} symmetry, in order of increasing energy. Figures 1, 2 and Table 1 will serve as a reference for the subsequent discussion and interpretation of the resonances of pyrene.

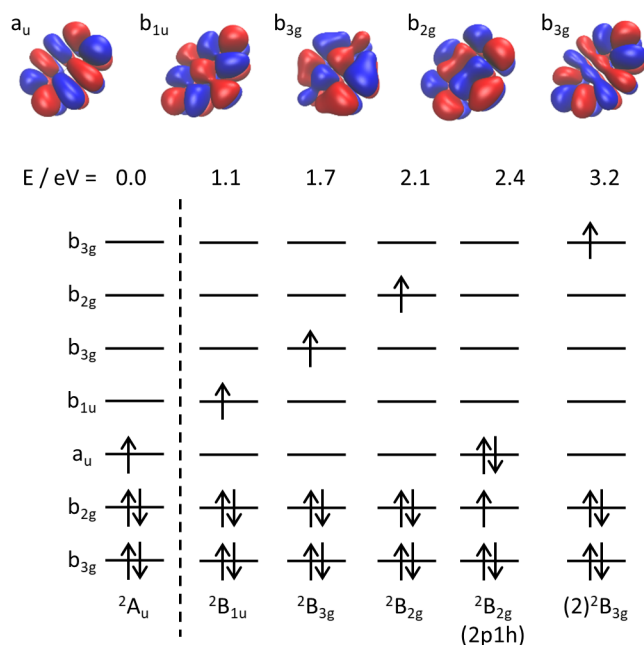


Figure 2: Relevant frontier molecular orbitals of pyrene and electronic configurations of its low-lying anion states. Energies of excited states are given relative to the anion ground 2A_u ground state; relative to the neutral ground state, these would be 0.4 eV lower in energy.

Discussion

The 2D PE spectrum of the gas-phase anion gives transition energies of 1.1, 2.1, 2.4, 3.2 and 3.8 eV. As seen from Table 1, all of these agree to within ~ 0.1 eV with transitions observed in the matrix isolation spectrum of Shida and Iwata. The latter also displays a transition at 1.75 eV, which is not discernible in our gas-phase PE measurements. The transition energies obtained from the EOM calculations agree to within 0.2 eV with the experimental values, with the exception that the calculations fail to predict a transition near 2.5 eV. We believe that

this transition likely has considerable 2-particle one-hole (2p1h) character and thus is not adequately described with the EOM-CCSD method. The computations allow us to assign the observed transitions as indicated in Table 1.

The EOM-CCSD calculations unambiguously assign the ground state anion to 2A_u symmetry. Moreover, the calculations predict that at the geometry of the neutral the anion is bound by 0.17 eV, compared to the experimental value of 0.41 eV. The underbinding is due to the limitations of the basis set and high-order correlation effects not recovered in our calculations. The scattering calculations of Singh *et al.* fail to give a bound anion,²⁶ even though experiment clearly shows that it is bound. The same is true for their calculations on anthracene. It appears that all their anion states are too high in energy by about 1 eV. However, the energy differences between their ground state and the upper anion states are in good agreement with the assignments discussed above, except that the R-matrix calculations do not predict an excited anion state near 2.5 eV, providing further support that this resonance is 2p1h in nature.

We now briefly consider the predictions of the pairing theorem. In this analysis we make use of IP's of pyrene determined in the PE spectroscopic study of Mishra *et al.*⁶⁴ The assignment of the first four features in the PE spectrum as due to ionization from π orbitals appears on firm grounds, and indeed the first three anion excitation energies based on the experimental IP's and application of the pairing theorem agree to within 0.1 eV of transitions measured in the present study. The assignments of the higher energy cation states is less clear due the overlapping of bands due to ionization from π and σ orbitals and also configurations of 1p2h character. Nonetheless, we note that there are ionization bands that when combined with the pairing theorem predict anion states at 2.6 and 3.3 eV in good agreement with experiment.

In the following discussion we consider the excited resonance states of the anion in order of increasing energy.

1.2 eV ${}^2B_{1u}$ resonance

The lowest energy resonance observed in the 2D PE spectrum around $1.0 < h\nu < 1.5$ eV is assigned to the ${}^2B_{1u}$ state. Although the ${}^2B_{1u} \leftarrow {}^2A_u$ transition is symmetry forbidden, it is clear from the absorption spectrum, both in the gas phase and in the matrix isolation experiments, that it is populated optically. The acquired intensity is likely due to vibronic coupling with the energetically nearby ${}^2B_{3g}$ and ${}^2B_{2g}$ anion states, discussed below. While the 2D PE

spectrum in this range shows a peak that is consistent with a direct detachment channel, there is also signal at very low eKE which arises from thermionic emission. This is more clearly seen in the $h\nu = 1.25$ eV PE spectrum shown in Figure 3(a). The appearance of thermionic emission indicates that one of the decay channels of this resonance is internal conversion to form the X^2A_u ground state of the anion. The details of the internal conversion mechanism have not been studied here, but could be probed through time-resolved photoelectron spectroscopy.^{53,54}

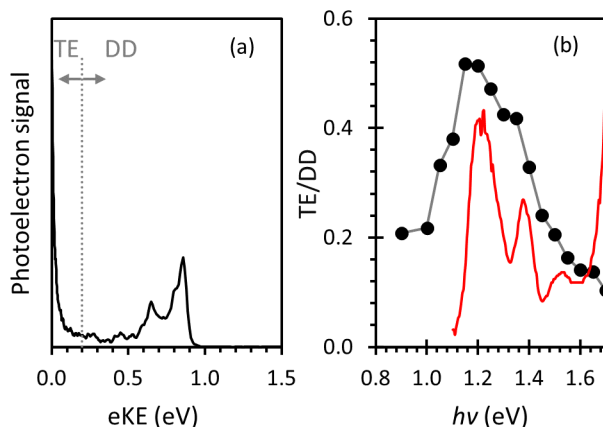


Figure 3: (a) Photoelectron spectrum taken at $h\nu = 1.20$ eV, showing direct detachment (DD) and thermionic emission (TE) at low electron kinetic energy (eKE). (b) Ratio of integrated photoelectron signal arising from TE and DD (full circles and grey line) along with the matrix isolation absorption spectrum (red line) that was adapted with permission from ref. 24. Copyright 1973 American Chemical Society.

The absorption (action) profile for the ${}^2B_{1u} \leftarrow {}^2A_u$ transition can be crudely recovered from the 2D PE spectrum by taking the ratio of the integrated thermionic emission signal to the integrated signal of direct detachment (TE and DD, respectively, in Figure 3(a)). This correspondence between the ratio and absorption spectrum is valid if all the resonance population decays to produce TE and if the yield of electrons in the DD channel remains constant with changing $h\nu$. The results of such an analysis are shown in Figure 3(b). The overall agreement with the absorption spectrum of Shida and Iwata is excellent, although we cannot determine the fraction of population that decays by internal conversion. From Figure 3(b), we find the absorption maximum to be at $h\nu = 1.2$ eV. Our estimate of the resonance position based on the onset of the thermionic emission ($h\nu \sim 1.1$ eV, Table 1) highlights the uncertainty in obtaining resonance positions using this strategy. From Figure 3(b) it is seen that in the spectrum obtained in the matrix, there is a well-resolved progression with spacing of about 1600 cm^{-1} , which is expected to

correspond to a C–C stretch vibration. There is also some evidence of vibrational structure in the action spectrum, suggesting that the lifetime for autodetachment is long enough to allow non-adiabatic dynamics to compete with electron loss.⁵³ Indeed, the scattering calculations by Singh *et al.* predict the ${}^2B_{1u}$ to be the longest lived of their predicted resonances (see Table 1). However, we stress that the action spectrum is a crude measure of the absorption. This is due, in part, to the fact that in our experiment electrons are only collected over a ~ 200 ns window. Thermionic emission can take significantly longer than this and, therefore, the yield of thermionic emission observed in the spectra is likely to be significantly lower than the true thermionic emission signal. The observation of regeneration of the ground state anion at low energy is significant from an astronomical perspective^{63,65} as briefly commented on below.

1.75 eV (1) ${}^2B_{3g}$ resonance

The next resonance is predicted to be of B_{3g} symmetry and appears near 1.75 eV in the absorption spectrum in the matrix isolation study. As noted above, this resonance is not distinguished in the present PE measurements. There are at least two reasons for this. Firstly, although the transition is optically allowed, it appears to have a rather low oscillator strength based on the absorption spectrum in the THF matrix. Secondly, if autodetachment is fast and the changes in Franck Condon factors between the ${}^2B_{3g}$ state and the X^2A_u state of the anion and the X^1A_g ground state of the neutral are similar, then the autodetachment spectrum may have a similar appearance as the direct detachment channel, thus making it difficult to identify. Note that Singh *et al.* do predict a short lifetime for this resonance (based on its width). Similar cases have been observed, with an example being para-benzoquinones.^{18,66} It is also important to recognise that the direct detachment spectrum that is unperturbed by resonances is not easily determined in the current experiment because of the very high density of resonances. This is likely to become even more problematic for larger PAH radical anions.

2.1 eV ${}^2B_{2g}$ resonance

The next anion state in order of increasing energy is of ${}^2B_{2g}$ symmetry, the transition to which is dipole-allowed from the 2A_u ground state. In the 2D PE spectrum, the transition is characterized by a clear change in the Franck-Condon envelope of the direct detachment feature. This change is exemplified in Figure 4, where the PE

spectra are plotted in the range $2.0 \leq h\nu \leq 2.6$ eV. The PE spectra are plotted in terms of the energy relative to the neutral ground state ($\nu = 0$), $E = h\nu - eKE - EA$, which should be viewed therefore as the energy remaining in the neutral following electron emission (or equivalent to electron energy loss). All spectra have been normalised to the height of the peak at lowest binding energy. It is clear that the electron is lost by autodetachment as there is no evidence of internal conversion to any of the lower-lying anion states. Singh *et al.* predict a very short lifetime for this resonance, which is consistent with this observation. Similar spectral changes have been seen in other molecular anions.^{20,67} Despite the changing Franck-Condon profile, the vibrational spacing remains consistent with excitation of C–C stretching modes in the final neutral X^1A_g state.

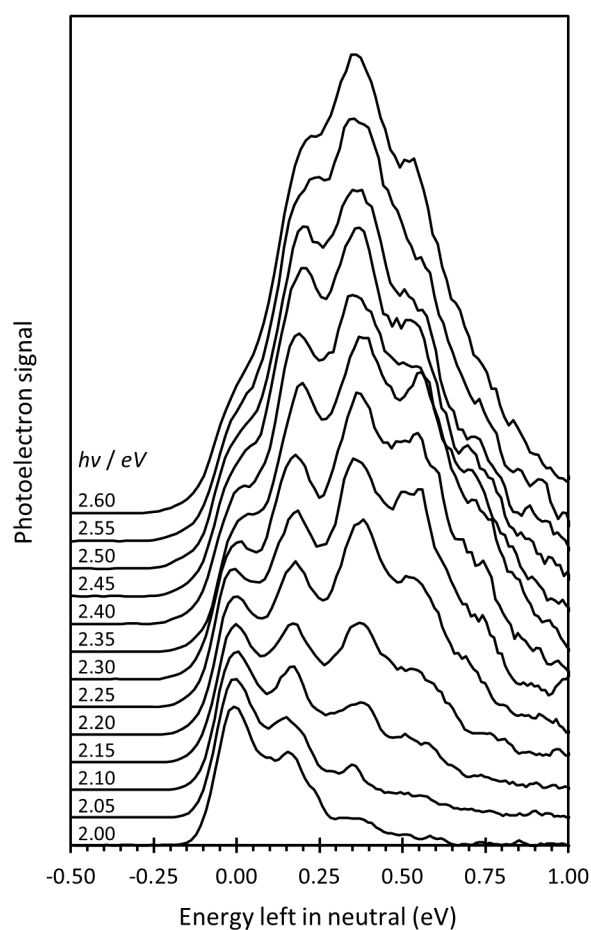


Figure 4: Photoelectron spectra taken in the range $2.0 \leq h\nu \leq 2.6$ eV, plotted in terms of energy relative to $\nu = 0$ of the neutral ground state, normalised to the height of the peak at lowest binding energy. These spectra highlight the changing Franck-Condon profile of the detachment feature.

2.4 eV $^2B_{2g}(2p1h)$ resonance

The next transition (at 2.4 and 2.49 eV in the PE and matrix isolation experiments, respectively) is 20 times more intense in the absorption spectrum than the lower energy transitions (peak not integrated intensity). This is consistent with the large oscillator strength associated with the singlet $b_{2g} \rightarrow a_u$ transition in the neutral molecule. Neither the EOM-CCSD calculations nor the R-matrix calculations predict a transition near this energy leading us to conclude that this state is largely 2p1h in character with the dominant electronic configuration $(b_{2g})^1(a_u)^2$. Anion states with a large 2p1h character are not well-described by the EOM-CCSD method. Interestingly, there is a peak in the PE spectrum of the neutral molecule near 10 eV, which if we assume applicability of the pairing theorem, predicts an excitation energy near 2.6 eV in the anion, consistent with the transition observed. Calculations have predicted that this cation state has considerable 1p2h character, while we anticipate that the species responsible for this feature in the anion spectrum is believed to be predominantly 2p1h in nature.

A new feature in Figure 1(b) with a constant central eKE ~ 1.8 eV correlates well with this transition. This is shown in more detail in Figure 5, for the range $2.5 \leq h\nu \leq 3.0$ eV, where the PE spectra have been plotted in terms of energy remaining in the neutral after detachment (see Figure 4) and normalised to maximum intensity. The autodetachment feature from this resonance is most clearly visible at $h\nu = 3.00$ eV as a broad high binding energy shoulder to the autodetachment peak from the lower lying ${}^2B_{2g}$ resonance. Again, there is no evidence of thermionic emission and the electron is lost by autodetachment, forming the ground state of the neutral. A puzzling aspect of this resonance is that, based on its electronic configuration, one might expect the ${}^3B_{2u}$ state to be a dominant decay channel, but this is not observed in Figure 1(b).

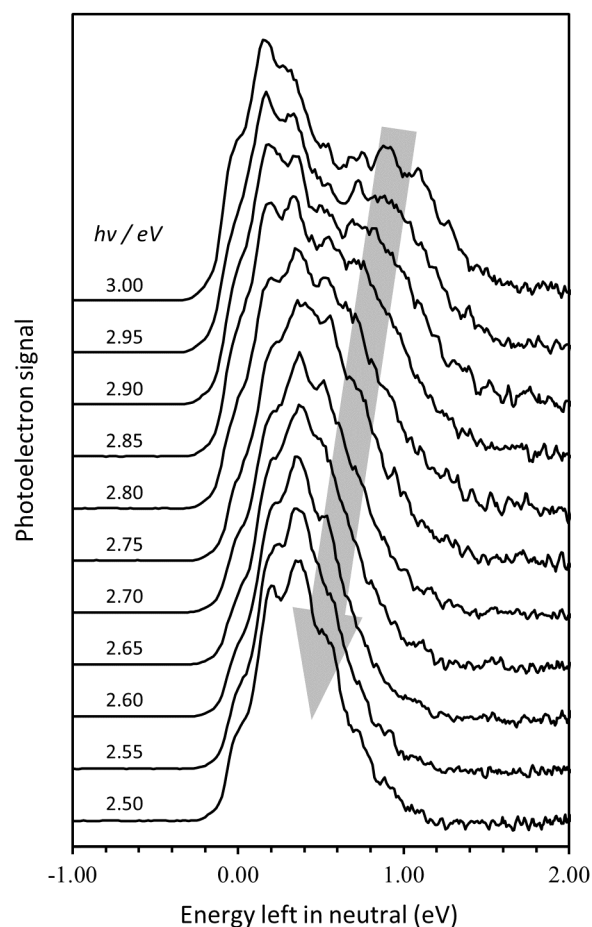


Figure 5: Photoelectron spectra taken in the range $2.5 \leq h\nu \leq 3.0$ eV, plotted in terms of energy relative to $v = 0$ of the neutral ground state, and normalised to maximum peak height. These spectra highlight the new emerging feature at low binding energy, which remains constant in terms of kinetic energy (as seen in Figure 1(b)).

3.2 eV (2^2B_{3g}) resonance

The next resonance observed occurs near 3.2 eV and is assigned to the second anion state of 2^2B_{3g} symmetry. The absorption spectrum has an excellent correlation with changes in the 2D PE spectrum at $h\nu \sim 3.2$ eV. The most obvious change is that there is a sudden increase in the formation of the final 3^3B_{3u} state upon electron loss. This observation suggests that this resonance has in addition to the $1p \dots (b_{2g})^2(a_u)^0(b_{1u})^0(b_{3g})^0(b_{2g})^0(b_{3g})^1$ configuration an admixture of the $2p1h \dots (b_{2g})^1(a_u)^1(b_{1u})^1(b_{3g})^0(b_{2g})^0(b_{3g})^0$. Our calculations confirm that this is the case with this configuration contributing about 10% to the wavefunction. Again, no thermionic emission is observed, indicating that

this resonance also decays exclusively by autodetachment. The R-matrix scattering calculations indicate that the width for this state is relatively narrow, consistent with the sharp onset of the resonance in the 2D PE spectrum.

Closer inspection of the region $3.2 < h\nu < 3.6$ eV in Figure 1(b) shows that there is a modulation of the PE signal for the ${}^1A_g + e^-$ detachment channel. Similar behavior was seen in the 2D PE spectrum of the anthracene anion.²¹ In that case, the modulation was assigned to a competition between resonance excitation and direct detachment. That is to say, when $h\nu$ is resonant with a vibrational level of the $(2) {}^2B_{3g} \leftarrow {}^2A_u$ transition, then the ratio of electrons emitted to the final neutral states, ${}^3B_{2u} : {}^1A_g$ will be different compared to when the excitation is not resonant (i.e., a larger direct than autodetachment contribution). Hence, the period of this modulation should reflect the spacing between vibrational levels in the absorption spectrum. In a similar spirit to Figure 3(b), in Figure 6, we have plotted the ratio of integrated intensities between the ${}^3B_{2u} + e^-$ and $X^1A_g + e^-$ channels, along with the absorption spectrum from Shida and Iwata in this range. Excellent agreement of the spacing of the vibrations in $(2) {}^2B_{3g} \leftarrow {}^2A_u$ absorption band with the modulation can be seen. Additionally, as shown in Figure 6, the absorption spectrum requires a blue-shift of ~ 60 meV to align with the gas-phase action spectrum. Such a shift is quite reasonable given the differing environments (gas-phase vs. matrix).

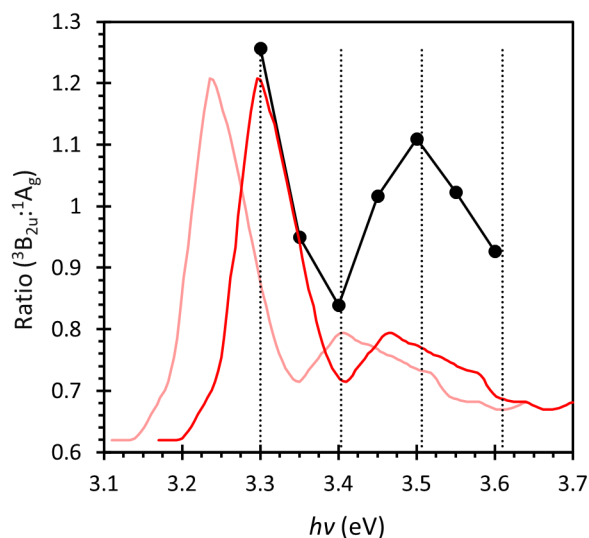


Figure 6: Ratio of integrated intensities between the ${}^3B_{2u}$ and 1A_g channels in the range $3.3 \leq h\nu \leq 3.6$ eV (solid black circles and grey line), along with the absorption spectrum (pale red line)²⁴ and the same spectrum blue-shifted by 60 meV (red line). Vertical dashed lines represent guides to the vibrational structure in the spectra. The absorption spectrum was adapted with permission from ref. 24. Copyright 1973 American Chemical Society.

Higher-lying resonances

Beyond the $(2)^2B_{3g} \leftarrow ^2A_u$ transition, there appears to be another change in the 2D PE spectrum around $h\nu = 3.8$ eV, with a much larger probability of forming the X^1A_g ground state compared to the $^3B_{2u}$ neutral state. The first singlet state of the neutral also becomes accessible at higher $h\nu$. We do not offer assertive interpretations of the dynamics or states involved in for these resonances because: (1) we do not have sufficient data spanning the higher $h\nu$ range; (2) there are many competing open decay channels which dramatically complicate the interpretations; (3) the density of resonances increases substantially at higher $h\nu$, which in particular involve a number electronic states with 2p1h character; and (4) we do not have the supporting absorption spectrum in this range.

Astronomical implications

As mentioned in the introduction, PAHs and low energy electrons are common in the interstellar medium.⁶⁸ In dense molecular clouds, it has been predicted that PAHs become the dominant carrier of negative charge instead of electrons.⁶⁹⁻⁷² This prediction is based on an expectation that PAHs with >30 carbon atoms efficiently capture low-energy electrons, while those with <30 carbon atoms do not. The dependence on number of C atoms in the PAH is motivated by the positive correlation between it and the PAH's EA. However, for pyrene, with only 16 C atoms and a relatively small EA, we show that low-energy electrons are also captured to form the ground state of the anion – at least over an energy range of about $0.6 < eKE < 1.1$ eV. Consequently, even pyrene might be quite effective at electron capture at low energies. Generally, it is the detailed chemical dynamics associated with the resonance decay that ultimately dictates the outcome of the electron-molecule reaction. Of course, once in the ground state, the electron will be emitted and the lifetime of this thermionic emission also depends on the number of C atoms. Specifically, more vibrational degrees of freedom leads to the excess energy being spread over more degrees of freedom, increasing the time for electron detachment. Nevertheless, the study presented here highlights that the empirical correlation is an over-simplified view of the complex dynamics that can lead to electron capture. 2D PE spectroscopy supported by computational chemistry as demonstrated here offers a route to understanding these dynamics in small PAHs. Indeed, small chemical changes to the PAH such as deprotonation,^{65,63} substitutions with heteroatoms,⁷³ or microsolvation⁷⁴ can dramatically alter the resonance dynamics and electron capture probabilities.

The role of microsolvation of PAHs, in particular, is likely to be important from an astronomical perspective because of the incorporation of PAHs in icy grains and dust in dense molecular clouds. In a recent experiment, we have shown the effect of solvation on the resonance dynamics of anthracene.⁷⁴ This revealed that the addition of a certain number of water molecules led to the lowest resonance becoming a bound state as the EA increases and that this dramatically increased the yield of thermionic emission. Given the proximity of the $^2B_{1u}$ resonance to threshold, and the fact that it already shows some thermionic emission, it is reasonable to expect that solvation might increase the ground state formation for electron capture by pyrene at low eKE. Conversely, however, there are no higher-lying resonances that decay into the lowest resonance. This contrasts to observations in the anthracene anion where excitation to certain resonances led to decay into the lowest energy resonance. Ongoing experiments are exploring the effect of solvent clusters on the low-lying resonances of pyrene.

Conclusions

The low energy electronic resonances in pyrene have been studied by 2D photoelectron imaging of the pyrene anion and by electronic structure computational methods that avoid collapse of the resonance onto discretized continuum states. Our results are in good agreement with a previous absorption spectrum of the pyrene anion in a glass, with electron-scattering calculations once a static shift of 1 eV was applied, and when applying the pairing theorem. Taken together, our results provide an assignment of the first five resonances in pyrene.

Most of the observed resonances decay exclusively by autodetachment and signatures of these dynamics are clearly seen in the 2D photoelectron spectrum. However, the photoelectron spectra resonant with the lowest lying $^2B_{1u}$ anion state show that electrons are emitted by thermionic emission, thus evidencing that this resonance decays by internal conversion to the ground state of the anion. From an astronomical perspective, PAHs are common in dense molecular clouds but are only considered to be effective at capturing low energy electrons when 30 or more carbon atoms are present. Our results show that pyrene, with only 14 C atoms can capture an electron via the $^2B_{1u}$ resonance.

Acknowledgement

AL and JRRV thank the ESPRC for funding (grant EP/R023085/1). SS and KDJ acknowledge support from the US National Science Foundation under grant number CHE1762337. The calculations were carried out on computers in the University of Pittsburgh's Center for Research Computing.

References

- (1) Dewar, M. J. S. A Molecular Orbital Theory of Organic Chemistry. I. General Principles. *J. Am. Chem. Soc.* **1952**, *74* (13), 3341–3345.
- (2) Dewar, M. J. S. A Molecular Orbital Theory of Organic Chemistry. II.1 The Structure of Mesomeric Systems. *J. Am. Chem. Soc.* **1952**, *74* (13), 3345–3350.
- (3) Förster, T.; Kasper, K. Ein Konzentrationsumschlag der Fluoreszenz des Pyrens. *Z. Für Elektrochem. Berichte Bunsenges. Für Phys. Chem.* **1955**, *59* (10), 976–980.
- (4) Kalyanasundaram, K.; Thomas, J. K. Environmental Effects on Vibronic Band Intensities in Pyrene Monomer Fluorescence and Their Application in Studies of Micellar Systems. *J. Am. Chem. Soc.* **1977**, *99* (7), 2039–2044.
- (5) Birks, J. B. Photophysics of Aromatic Molecules. *Wiley-Interscience, London*, **1970**.
- (6) Figueira-Duarte, T. M.; Müllen, K. Pyrene-Based Materials for Organic Electronics. *Chem. Rev.* **2011**, *111* (11), 7260–7314.
- (7) Tielens, A. G. G. M. The Molecular Universe. *Rev. Mod. Phys.* **2013**, *85* (3), 1021–1081.
- (8) Tielens, A. G. G. M. Interstellar Polycyclic Aromatic Hydrocarbon Molecules. *Annu. Rev. Astron. Astrophys.* **2008**, *46* (1), 289–337.
- (9) Vijh, U. P.; Witt, A. N.; Gordon, K. D. Small Polycyclic Aromatic Hydrocarbons in the Red Rectangle. *Astrophys. J.* **2005**, *619* (1), 368.
- (10) Ando, N.; Kokubo, S.; Mitsui, M.; Nakajima, A. Photoelectron Spectroscopy of Pyrene Cluster Anions, (Pyrene) N^- ($N=1-20$). *Chem. Phys. Lett.* **2004**, *389* (4), 279–283.

- (11) Schulz, G. J. Resonances in Electron Impact on Diatomic Molecules. *Rev. Mod. Phys.* **1973**, *45* (3), 423–486.
- (12) Christophorou, L. G. *Electron–Molecule Interactions and Their Applications*; Academic Press, 1984.
- (13) Jordan, K. D.; Burrow, P. D. Temporary Anion States of Polyatomic Hydrocarbons. *Chem. Rev.* **1987**, *87* (3), 557–588.
- (14) Allan, M. Study of Triplet States and Short-Lived Negative Ions by Means of Electron Impact Spectroscopy. *J. Electron Spectrosc. Relat. Phenom.* **1989**, *48* (2), 219–351.
- (15) Reddish, T.; Currell, F.; Comer, J. Studies of the 2 eV Shape Resonance in N₂ using a Two-Dimensional Scanning Technique. *J. Phys. [E]* **1988**, *21* (2), 203–207.
- (16) Currell, F.; Comer, J. Observation of Friction in the Nuclear Dynamics of CO₂⁻ near the Equilibrium Geometry of the Negative Ion. *Phys. Rev. Lett.* **1995**, *74* (8), 1319–1322.
- (17) Regeta, K.; Allan, M. Autodetachment Dynamics of Acrylonitrile Anion Revealed by Two-Dimensional Electron Impact Spectra. *Phys. Rev. Lett.* **2013**, *110* (20), 203201.
- (18) West, C. W.; Bull, J. N.; Antonkov, E.; Verlet, J. R. R. Anion Resonances of Para-Benzoquinone Probed by Frequency-Resolved Photoelectron Imaging. *J. Phys. Chem. A* **2014**, *118* (48), 11346–11354.
- (19) Anstöter, C. S.; Bull, J. N.; Verlet, J. R. R. Ultrafast Dynamics of Temporary Anions Probed through the Prism of Photodetachment. *Int. Rev. Phys. Chem.* **2016**, *35* (4), 509–538.
- (20) Anstöter, C. S.; Mensa-Bonsu, G.; Nag, P.; Ranković, M.; Kumar T. P., R.; Boichenko, A. N.; Bochenkova, A. V.; Fedor, J.; Verlet, J. R. R. Mode-Specific Vibrational Autodetachment Following Excitation of Electronic Resonances by Electrons and Photons. *Phys. Rev. Lett.* **2020**, *124* (20), 203401.

- (21) Mensa-Bonsu, G.; Lietard, A.; Tozer, D. J.; Verlet, J. R. R. Low Energy Electron Impact Resonances of Anthracene Probed by 2D Photoelectron Imaging of Its Radical Anion. *J. Chem. Phys.* **2020**, *152* (17), 174303.
- (22) Kim, J. H.; Lee, S. H.; Song, J. K. Photoelectron Spectroscopy of Pyrene Anion Clusters: Autodetachment via Excited States of Anion and Intermolecular Interactions in Anion Clusters. *J. Chem. Phys.* **2009**, *130* (12), 124321.
- (23) Zahradnik, R.; Carsky, P. Conjugated Radicals. II. Semiempirical Calculations of Electronic Spectra of Radical Anions Derived from Alternant Hydrocarbons. *J. Phys. Chem.* **1970**, *74* (6), 1240–1248.
- (24) Shida, Tadamasa.; Iwata, Suehiro. Electronic Spectra of Ion Radicals and Their Molecular Orbital Interpretation. III. Aromatic Hydrocarbons. *J. Am. Chem. Soc.* **1973**, *95* (11), 3473–3483.
- (25) Carlson, B. J.; Falcetta, M. F.; Slimak, S. R.; Jordan, K. D. A Fresh Look at the Role of the Coupling of a Discrete State with a Pseudocontinuum State in the Stabilization Method for Characterizing Metastable States. *J. Phys. Chem. Lett.* **2021**, *12* (4), 1202–1206.
- (26) Singh, S.; Gupta, D.; Antony, B.; Tudorovskaya, M.; Tennyson, J. Electron Scattering Cross Sections for Anthracene and Pyrene. *J. Phys. Chem. A* **2020**, *124* (35), 7088–7100.
- (27) Rogers, J. P.; Anstöter, C. S.; Bull, J. N.; Curchod, B. F. E.; Verlet, J. R. R. Photoelectron Spectroscopy of the Hexafluorobenzene Cluster Anions: $(C_6F_6)N^-$ ($n = 1 - 5$) and $I-(C_6F_6)$. *J. Phys. Chem. A* **2019**, *123* (8), 1602–1612.
- (28) Wiley, W. C.; McLaren, I. H. Time-of-Flight Mass Spectrometer with Improved Resolution. *Rev. Sci. Instrum.* **1955**, *26* (12), 1150–1157.
- (29) Eppink, A. T. J. B.; Parker, D. H. Velocity Map Imaging of Ions and Electrons Using Electrostatic Lenses: Application in Photoelectron and Photofragment Ion Imaging of Molecular Oxygen. *Rev. Sci. Instrum.* **1997**, *68* (9), 3477–3484.

- (30) Roberts, G. M.; Nixon, J. L.; Lecointre, J.; Wrede, E.; Verlet, J. R. R. Toward Real-Time Charged-Particle Image Reconstruction Using Polar Onion-Peeling. *Rev. Sci. Instrum.* **2009**, *80* (5), 053104.
- (31) Hazi, A. U.; Taylor, H. S. Stabilization Method of Calculating Resonance Energies: Model Problem. *Phys. Rev. A* **1970**, *1* (4), 1109–1120.
- (32) Riss, U. V.; Meyer, H.-D. Calculation of Resonance Energies and Widths Using the Complex Absorbing Potential Method. *J. Phys. B At. Mol. Opt. Phys.* **1993**, *26* (23), 4503–4535.
- (33) Jagau, T.-C.; Bravaya, K. B.; Krylov, A. I. Extending Quantum Chemistry of Bound States to Electronic Resonances. *Annu. Rev. Phys. Chem.* **2017**, *68* (1), 525–553.
- (34) Balslev, E.; Combes, J. M. Spectral Properties of Many-Body Schrödinger Operators with Dilatation-Analytic Interactions. *Commun. Math. Phys.* **1971**, *22* (4), 280–294.
- (35) Simon, B. Resonances and Complex Scaling: A Rigorous Overview. *Int. J. Quantum Chem.* **1978**, *14* (4), 529–542.
- (36) McCurdy, C. W.; Rescigno, T. N. Extension of the Method of Complex Basis Functions to Molecular Resonances. *Phys. Rev. Lett.* **1978**, *41* (20), 1364–1368.
- (37) Stanton, J. F.; Gauss, J. Perturbative Treatment of the Similarity Transformed Hamiltonian in Equation-of-motion Coupled-cluster Approximations. *J. Chem. Phys.* **1995**, *103* (3), 1064–1076.
- (38) Dunning, T. H. Gaussian Basis Sets for Use in Correlated Molecular Calculations. I. The Atoms Boron through Neon and Hydrogen. *J. Chem. Phys.* **1989**, *90* (2), 1007–1023.
- (39) Becke, A. D. Density-functional Thermochemistry. III. The Role of Exact Exchange. *J. Chem. Phys.* **1993**, *98* (7), 5648–5652.
- (40) Lee, C.; Yang, W.; Parr, R. G. Development of the Colle-Salvetti Correlation-Energy Formula into a Functional of the Electron Density. *Phys. Rev. B* **1988**, *37* (2), 785–789.
- (41) Vosko, S. H.; Wilk, L.; Nusair, M. Accurate Spin-Dependent Electron Liquid Correlation Energies for Local Spin Density Calculations: A Critical Analysis. *Can. J. Phys.* **2011**.

- (42) Stephens, P. J.; Devlin, F. J.; Chabalowski, C. F.; Frisch, M. J. Ab Initio Calculation of Vibrational Absorption and Circular Dichroism Spectra Using Density Functional Force Fields. *J. Phys. Chem.* **1994**, *98* (45), 11623–11627.
- (43) Krishnan, R.; Binkley, J. S.; Seeger, R.; Pople, J. A. Self-consistent Molecular Orbital Methods. XX. A Basis Set for Correlated Wave Functions. *J. Chem. Phys.* **1980**, *72* (1), 650–654.
- (44) Frisch, M. J.; Trucks, G. W.; Schlegel, H. B.; Scuseria, G. E.; Robb, M. A.; Cheeseman, J. R.; Scalmani, G.; Barone, V.; Petersson, G. A.; Nakatsuji, H.; *et al.* *Gaussian 16, Revision C.01*, Gaussian, Inc., Wallingford CT, 2016.
- (45) Matthews, D. A.; Cheng, L.; Harding, M. E.; Lipparini, F.; Stopkowitz, S.; Jagau, T.-C.; Szalay, P. G.; Gauss, J.; Stanton, J. F. Coupled-Cluster Techniques for Computational Chemistry: The CFOUR Program Package. *J. Chem. Phys.* **2020**, *152* (21), 214108.
- (46) Coulson, C. A.; Rushbrooke, G. S. Note on the Method of Molecular Orbitals. *Math. Proc. Camb. Philos. Soc.* **1940**, *36* (2), 193–200.
- (47) Burrow, P. D.; Michejda, J. A.; Jordan, K. D. Experimental Study of the Negative Ion States of Styrene. A Test of the Pairing Theorem. *J. Am. Chem. Soc.* **1976**, *98* (20), 6392–6393.
- (48) Jordan, K. D.; Burrow, P. D. On the Relationship between the Gas Phase, Condensed Phase and Theoretical Spectra of Alternant Hydrocarbon Anions. *Chem. Phys.* **1980**, *45* (2), 171–182.
- (49) Nemeth, G. I.; Selzle, H. L.; Schlag, E. W. Magnetic ZEKE Experiments with Mass Analysis. *Chem. Phys. Lett.* **1993**, *215* (1), 151–155.
- (50) Burrow, P. D.; Michejda, J. A.; Jordan, K. D. Electron Transmission Study of the Temporary Negative Ion States of Selected Benzenoid and Conjugated Aromatic Hydrocarbons. *J. Chem. Phys.* **1987**, *86* (1), 9–24.
- (51) Mangle, E. A.; Topp, M. R. Excited-State Dynamics of Jet-Cooled Pyrene and Some Molecular Complexes. *J. Phys. Chem.* **1986**, *90* (5), 802–807.

- (52) Borisevich, N. A.; Vodovatov, L. B.; D'yachenko, G. G.; Petukhov, V. A.; Semyonov, M. A. Fluorescence of Free Pyrene Molecules Cooled in a Supersonic Jet. *J. Appl. Spectrosc.* **1995**, *62* (3), 482–488.
- (53) Horke, D. A.; Li, Q.; Blancafort, L.; Verlet, J. R. R. Ultrafast Above-Threshold Dynamics of the Radical Anion of a Prototypical Quinone Electron-Acceptor. *Nat. Chem.* **2013**, *5* (8), 711–717.
- (54) Bull, J. N.; West, C. W.; Verlet, J. R. R. On the Formation of Anions: Frequency-, Angle-, and Time-Resolved Photoelectron Imaging of the Menadione Radical Anion. *Chem. Sci.* **2015**, *6* (2), 1578–1589.
- (55) Campbell, E. E. B.; Levine, R. D. Delayed Ionization and Fragmentation En Route to Thermionic Emission: Statistics and Dynamics. *Annu. Rev. Phys. Chem.* **2000**, *51* (1), 65–98.
- (56) Andersen, J. U.; Bonderup, E.; Hansen, K. Thermionic Emission from Clusters. *J. Phys. B At. Mol. Opt. Phys.* **2002**, *35* (5), R1.
- (57) Adams, C. L.; Hansen, K.; Weber, J. M. Vibrational Autodetachment from Anionic Nitroalkane Chains: From Molecular Signatures to Thermionic Emission. *J. Phys. Chem. A* **2019**, *123* (40), 8562–8570.
- (58) Cooper, J.; Zare, R. N. Angular Distribution of Photoelectrons. *J. Chem. Phys.* **1968**, *48* (2), 942–943.
- (59) Reid, K. L. Photoelectron Angular Distributions. *Annu. Rev. Phys. Chem.* **2003**, *54* (1), 397–424.
- (60) Sanov, A. Laboratory-Frame Photoelectron Angular Distributions in Anion Photodetachment: Insight into Electronic Structure and Intermolecular Interactions. *Annu. Rev. Phys. Chem.* **2014**, *65* (1), 341–363.
- (61) Anstöter, C. S.; Verlet, J. R. R. Modeling the Photoelectron Angular Distributions of Molecular Anions: Roles of the Basis Set, Orbital Choice, and Geometry. *J. Phys. Chem. A* **2021**, *125* (22), 4888–4895.

- (62) Jagau, T.-C.; Dao, D. B.; Holtgrewe, N. S.; Krylov, A. I.; Mabbs, R. Same but Different: Dipole-Stabilized Shape Resonances in CuF⁻ and AgF⁻. *J. Phys. Chem. Lett.* **2015**, *6* (14), 2786–2793.
- (63) Stanley, L. H.; Anstöter, C. S.; Verlet, J. R. R. Resonances of the Anthracenyl Anion Probed by Frequency-Resolved Photoelectron Imaging of Collision-Induced Dissociated Anthracene Carboxylic Acid. *Chem. Sci.* **2017**, *8* (4), 3054–3061.
- (64) Mishra, P. M.; Avaldi, L.; Bolognesi, P.; Prince, K. C.; Richter, R.; Kadhane, U. R. Valence Shell Photoelectron Spectroscopy of Pyrene and Fluorene: Photon Energy Dependence in the Far-Ultraviolet Region. *J. Phys. Chem. A* **2014**, *118* (17), 3128–3135.
- (65) Bull, J. N.; West, C. W.; Verlet, J. R. R. Internal Conversion Outcompetes Autodetachment from Resonances in the Deprotonated Tetracene Anion Continuum. *Phys. Chem. Chem. Phys.* **2015**, *17* (48), 32464–32471.
- (66) Bull, J. N.; Verlet, J. R. R. Dynamics of Π^* -Resonances in Anionic Clusters of Para-Toluquinone. *Phys. Chem. Chem. Phys.* **2017**, *19* (39), 26589–26595.
- (67) Anstöter, C. S.; Gartmann, T. E.; Stanley, L. H.; Bochenkova, A. V.; Verlet, J. R. R. Electronic Structure of the Para-Dinitrobenzene Radical Anion: A Combined 2D Photoelectron Imaging and Computational Study. *Phys. Chem. Chem. Phys.* **2018**, *20* (37), 24019–24026.
- (68) Draine, B. T. Physics of the Interstellar and Intergalactic Medium. *Phys. Interstellar Intergalactic Medium Bruce T Draine Princet. Univ. Press 2011 ISBN 978-0-691-12214-4* **2011**.
- (69) Omont, A. Physics and Chemistry of Interstellar Polycyclic Aromatic Molecules. *Astron. Astrophys.* **1986**, *164*, 159–178.
- (70) Lepp, S.; Dalgarno, A. Polycyclic Aromatic Hydrocarbons in Interstellar Chemistry. *Astrophys. J.* **1988**, *324*, 553–556.

- (71) Allamandola, L. J.; Tielens, A. G. G. M.; Barker, J. R. Interstellar Polycyclic Aromatic Hydrocarbons - The Infrared Emission Bands, the Excitation/Emission Mechanism, and the Astrophysical Implications. *Astrophys. J. Suppl. Ser.* **1989**, *71*, 733–775.
- (72) Wakelam, V.; Herbst, E. Polycyclic Aromatic Hydrocarbons in Dense Cloud Chemistry. *Astrophys. J.* **2008**, *680*, 371–383.
- (73) K. Ashworth, E.; S. Anstöter, C.; R. Verlet, J. R.; N. Bull, J. Autodetachment Dynamics of 2-Naphthoxide and Implications for Astrophysical Anion Abundance. *Phys. Chem. Chem. Phys.* **2021**, *23* (10), 5817–5823.
- (74) Lietard, A.; Mensa-Bonsu, G.; Verlet, J. R. R. The Effect of Solvation on Electron Capture Revealed Using Anion Two-Dimensional Photoelectron Spectroscopy. *Nat. Chem.* **2021**, 1–6.